Kinetic ballooning modes driven turbulent transport in the inner core of JET H-mode plasmas

N. Kumar*, 1, 3, Y. Camenen[1], S. Benkadda[1], C. Bourdelle[2], A. Loarte[3], A.R. Polevoi [3], F.Widmer[1], and JET contributors**

[1] *Aix Marseille University, CNRS, PIIM UMR 7345, Marseille, France*

[2] *CEA, IRFM, Saint-Paul-lez-Durance, France*

[3] *ITER Organization, Route de Venon-sur Verdon, Saint-Paul-lez-Durance, France*

* *University of Colorado Boulder, Boulder, Colorado, US*

** *See the author list of "Overview of JET results for optimising ITER operation" by J. Mailloux et al. to be published in Nuclear Fusion Special issue: Overview and Summary Papers from the 28th Fusion Energy Conference (Nice, France, 10-15 May 2021)*

A reliable prediction of the temperature and density profile in the central region (ρ<0.3) of present and future magnetic fusion devices is crucial for the control of high-Z accumulation such as tungsten (W), which can lead to significant core radiation [1], and of the fusion performance. Turbulent transport in the central region remains, however, largely unexplored.

To better characterise turbulent transport and test the quasi-linear (QL) approximation in the central region, an extensive linear and nonlinear gyro-kinetic investigation has been carried out for JET hybrid H-mode discharge 75225 at ρ= 0.15 using the gyrokinetic code GKW [2] in the local approximation. This JET hybrid H-mode discharge was analysed in details for ρ=0.33 in [3,4,5]. The normalized local input parameters are shown in table 1. Despite lower gradients close to the magnetic axis, the plasma is found linearly unstable to the Kinetic Ballooning Mode (KBM) at ρ= 0.15 as shown in fig. 1 (a) and (b), consistently with [5]. These unstable modes are driven by the pressure gradient. The key parameters responsible for the KBM destabilisation in this region are the low magnetic shear and high-β values [6].

ρ	$\frac{R}{L_{Ti}}$	$\frac{R}{L_{Te}}$	$\frac{R}{L_{Tf}}$	$\frac{Te}{T_i}$	$\frac{T_f}{T_i}$	$\frac{R}{L_{ne}}$	$\frac{R}{L_{nf}}$	β_{ref} [%]	q	$\hat{s}$	u	u´	ν
0.15	4.2	1.9	1.8	0.69	5.6	1.5	0.80	4.6	1.10	0.05	0.31	0.59	0.015
0.33	7.7	4.1	9.6	0.84	6.1	2.7	8.97	2.6	1.14	0.21	0.32	1.31	0.019
0.60	5.9	5.5	9.6	1.05	4.6	3.3	7.96	1.0	1.74	1.42	0.24	0.24	0.034

Table 1: Normalized input parameters in GKW simulations for the JET 75225 discharge [6].

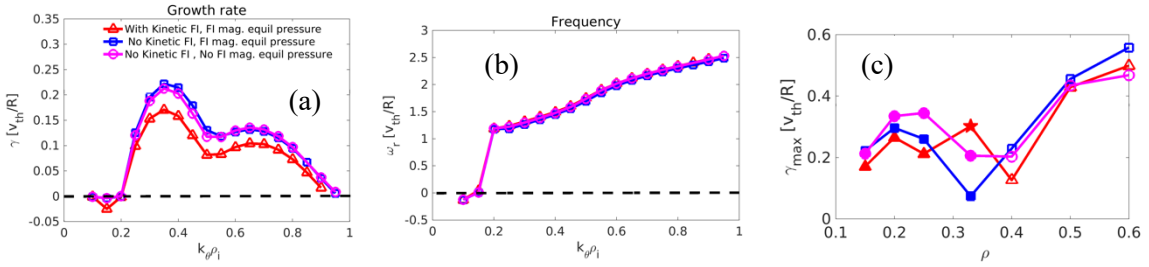

Fig. 1: Linear Growth rate (a) frequency (b) as function of $k_\theta \rho_i$ at radial location $\rho = 0.15$, and growth rate of the most unstable modes as a function of radial location ρ (c), for JET discharge 75225. The magenta curve is for the case without kinetic fast ions and without fast ion pressure in the magnetic equilibrium. The blue line correspond to the case without kinetic fast ions but the magnetic equilibrium includes the fast ion pressure. The red curve indicates the case with kinetic fast ions and fast ion pressure in the magnetic equilibrium[6].

Including fast ions as a kinetic species decreases the KBMs growth rate by about 20% (red curve), whereas the fast ion pressure in the magnetic equilibrium has almost no impact on the

mode growth rate (blue curve). At ρ=0.15, stable micro-tearing modes (MTM) are also obtained at the lowest $k_\theta \rho_i$, characterised by their negative frequency and the even parity of the vector potential fluctuations. In the present case, these MTMs are linearly stable but will matter for the QL analysis. Moreover, KBM is the dominant instability in the inner core $\rho < 0.4$ (full symbol), at mid and outer radius ($\rho > 0.4$) it changes to ITG (open symbol) as shown in figure 1 (c).

Following an in-depth analysis of the linear stability, nonlinear simulations are performed at ρ=0.15 with no kinetic fast ions and $E \times B$ shear. The corresponding time-dependent nonlinear (NL) heat fluxes for the experimental input values of magnetic shear and plasma beta are shown in figure 2. As seen here, the $\boldsymbol{E} \times \boldsymbol{B}$ contribution to the ion heat flux is found to be dominant, whereas, for the electron heat flux, a significant magnetic flutter contribution to the nonlinear heat flux is observed with a sign opposite to that obtained in linear simulations. This large contribution arises from stable micro-tearing modes (MTMs) at $k_\theta \rho_i$<0.2 that are excited nonlinearly.

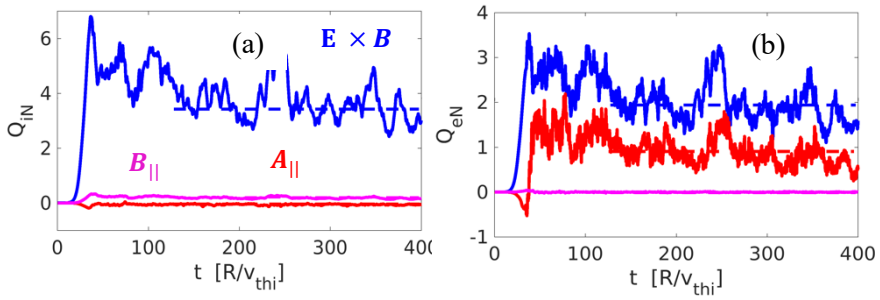

Fig. 2: Time trace of nonlinear ion (a) and electron heat flux (b) for JET 75225 at ρ=0.15. The blue curve is for ES, red for magnetic flutter and magenta is for magnetic compression contribution to the total NL heat flux [6].

Nonlinearly, the excitation of KBMs drives heat and particle fluxes increasing with higher beta (figure 3), consistently with the linear results. The nonlinear turbulent particle fluxes generated by KBMs are positive and outward-directed, with higher E × B contribution agreeing with linear particle fluxes ratios.

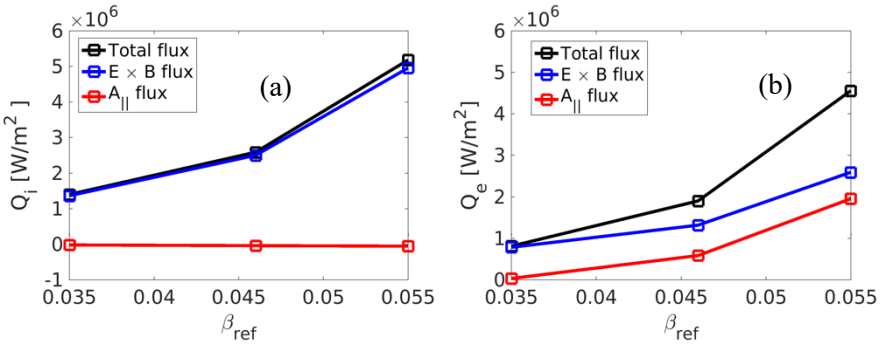

Fig. 3: The nonlinear ion (a) and electron heat flux (b) as function of β_{ref} for JET 75225 at ρ=0.15. The blue curve is for ES, red for magnetic flutter, and black curve is the total nonlinear heat flux [6].

The validity of standard reduced quasi-linear (QL) models employed in standard QL codes is then tested. The QL approximation assumes that the phase difference between fluctuating fields (e.g. n and ϕ for the $E \times B$ particle flux) is similar in the linear and the nonlinear regimes. When this approximation holds, the QL fluxes can be computed as: $Q^{QL}_{s,E\times B} = \sum_{k_r,k_\theta} Q^N_{s,E\times B}\, \mathcal{A}^2_{QL}$ and $Q^{QL}_{s,A_{||}} = \sum_{k_r,k_\theta} Q^N_{s,A_{||}}\, \mathcal{A}^2_{QL}$, with the first term on the right-hand side is the flux normalized to the mode amplitude obtained in linear simulations, $Q^N_S = Q_S/\mathcal{A}^2_L$, and the second term is an approximation of the nonlinear saturation amplitude: $\mathcal{A}_{QL} \sim \mathcal{A}_{NL}$. The mode amplitude in linear runs is defined as: $\mathcal{A}_L(k_r, k_\theta, t) = \sqrt{\int [\,|\phi|^2 + |A_{||}|^2 + |B_{||}|^2\,] ds \,/\, \int ds}$, where s is the parallel coordinate and the integral is performed over the full flux-tube domain. Three different QL models are tested in this work.

(1) **Mixing length model [7]:** in this model saturated mode amplitude is defined as: $W_1 = \mathcal{A}_{QL}^2 = C_1 \max\left[\frac{\gamma}{\langle k_\perp^2 \rangle}, 0\right]$. Here, $\langle k_\perp^2 \rangle$ is an effective perpendicular wavevector defined as:$\langle k_\perp^2 \rangle = \int k_\perp^2 |\phi|^2 ds / \int |\phi|^2 ds$. The main drawback of this model is that linearly stable modes will never contribute to the QL fluxes. (2) **QuaLiKiz model [8, 9]:** In this, the saturated mode amplitude is approximated by: $W_n = C_n S_k \max\left[\frac{\gamma}{\langle k_\perp^2 \rangle}\right] \frac{1}{k_\theta \rho_i^{max}}$, with $S_k = \left(\frac{k_\theta \rho_i}{k_\theta \rho_i^{max}}\right)^{x_n}$ for $k_\theta \rho_i < k_\theta \rho_i^{max}$ and $S_k = \left(\frac{k_\theta \rho_i}{k_\theta \rho_i^{max}}\right)^{-3}$ for $k_\theta \rho_i > k_\theta \rho_i^{max}$. Where $k_\theta \rho_i^{max}$ is the wave vector at max($\frac{\gamma}{\langle k_\perp^2 \rangle}$). Here, two different spectral shapes is tested: W_2 and W_3 with $x_2 = 1$ and $x_3 = 2$, to highlight the sensitivity of the magnetic flutter fluxes to the spectral rule used at low $k\theta\rho_i$. The unique constants C_1, C_2 and C_3 are set by matching the ion heat flux in the nonlinear simulation performed at nominal parameters.

The quasi-linear heat fluxes obtained with the quasi-linear models W_1 ,W_2 and W_3 are compared with the nonlinear fluxes with scalar multiplication factor of $C_1 = 12.4$, $C_2 = 4.24$ and $C_3 = 4.32$. At ρ= 0.15, the QL fluxes are in good agreement with nonlinear fluxes for the $\boldsymbol{E} \times \boldsymbol{B}$ contributions with some departure at high β as shown in figure 4 (ion heat fluxes have a similar trend and the figure is not shown here). However, these models fail to capture the magnetic flutter contribution to the electron heat flux (fig. 5) due to the nonlinearly excited MTMs with the mixing length model W_1 strongly underestimates the magnetic flutter contribution. In contrast, QuaLiKiz model W_2 and W_3 strongly overestimates the magnetic flutter heat flux.

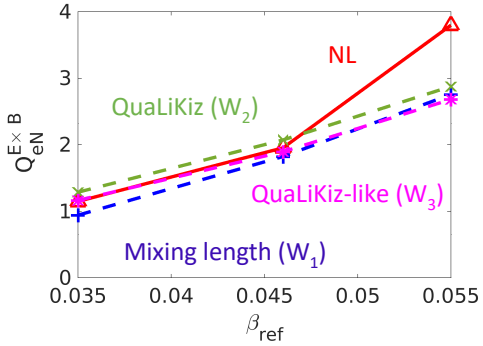

Fig. 4: $E \times B$ electron heat flux as function of β_{ref} for JET 75225 at ρ=0.15. The red curve is NL flux, blue for QL model W_1, green for W_2 and magenta for W_3 [6].

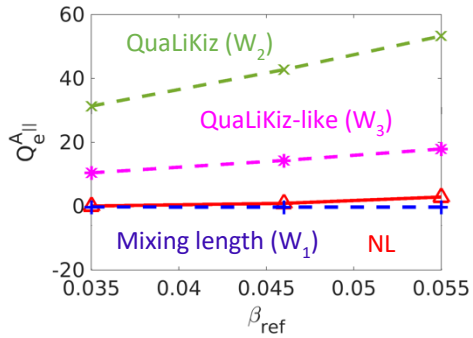

Fig. 5: Magnetic flutter electron ion heat flux as function of β_{ref} for JET 75225 at ρ=0.15. The red curve is NL flux, blue for QL model W_1, green for W_2 and magenta for W_3 [6].

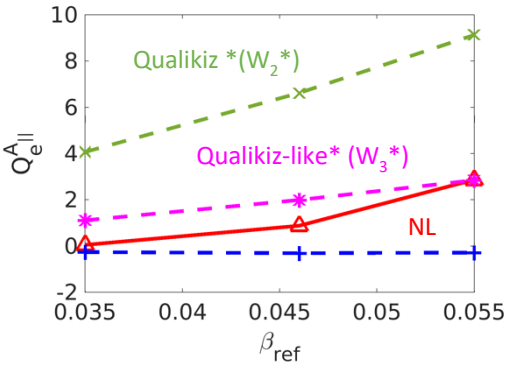

Fig. 6: Magnetic flutter electron ion heat flux as function of β_{ref} for JET 75225 at ρ=0.15. The red curve is NL flux, blue for QL model W_1, green for W_2^* and magenta for W_3^* [6].

This discrepancy is because of the ratio of the $A_{||}$ fluctuations amplitude to the total fluctuation amplitude at $k_\theta \rho_i = 0.1$ in linear runs is 10 times larger than the nonlinear one [6]. Linearly this ratio ($\mathcal{A}^2{}_{\mathcal{A}_{||}}/\mathcal{A}^2$) at low $k_\theta \rho_i$ is governed by the most unstable mode (MTM in present case). To capture this effect in QuaLiKiz-like QL model, an extra normalisation of the magnetic flutter fluxes in linear runs is introduced. First assume that: $\frac{\mathcal{A}_{A_{||},NL}}{\mathcal{A}_{NL}} \sim \frac{\mathcal{A}_{A_{||},L}(k_\theta \rho_i^{max})}{\mathcal{A}_L(k_\theta \rho_i^{max})}$, and then introducing the following quantity: $A_{||}^{ratio} = \frac{\mathcal{A}_L(k_\theta \rho_i)}{\mathcal{A}_{A_{||},L}(k_\theta \rho_i)} \frac{\mathcal{A}_{A_{||},L}(k_\theta \rho_i^{max})}{\mathcal{A}_L(k_\theta \rho_i^{max})}$ which is used to renormalise the amplitude of $\mathcal{A}_{||}$ in the

magnetic flutter fluxes as: $Q^{QL}_{s,\ A_{||}} = \sum_{k_r,\,k_\theta} Q^{N}_{s,\,A_{||}}\,\mathcal{A}^2_{QL}A^{ratio}_{||}$. This model is called as W_2^* and W_3^* and is compared with the nonlinear results in figure 6. The renormalisation of $A_{\|}$ in the linear magnetic flutter fluxes makes the prediction of the QuaLiKiz-like model much closer to the values of the fluxes obtained in the nonlinear simulations, in particular for $W_3{}^*$. Still, further work is required to improve the model.

The experimental power balance values for the nominal experimental parameters at ρ=0.15 are $Q_i^{Exp} = 47 \times 103\ W/m^2$, $Q_e^{Exp} = 16 \times 103\ W/m^2$, $\Gamma_e^{Exp} = 3.6 \times 1018\ m^{-2}\ s^{-1}$, these are two orders of magnitude smaller than the computed nonlinear outward electron particle and heat flux values for electron and ion. The QL model W_3 was used to test the sensitivity of these fluxes to the KBM drives and shown in figure 7.

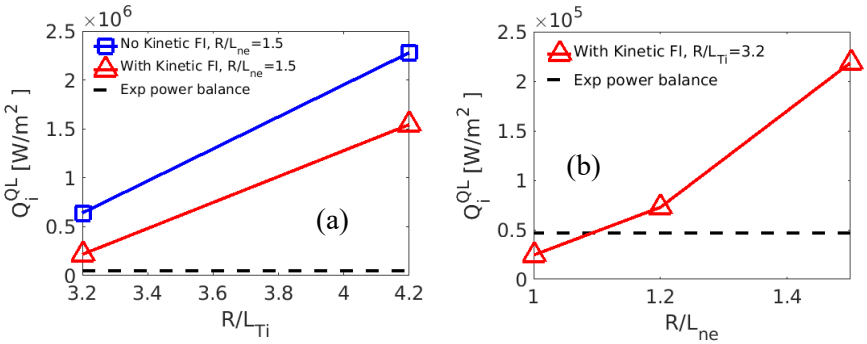

Fig. 7: Quasilinear ion heat flux as function of R/L_{Ti} (a) and R/L_{ne} for JET 75225 at ρ=0.15. The red curve is for the case with kinetic fast ion, blue without kinetic fast ion and dotted black line is experimental power balance heat fluxes value.

As seen here, a decrease of R/LTi and R/Ln by about 20% was sufficient to match the experimental fluxes, demonstrating the strong sensitivity to the input gradients. Finally, the QL turbulent W transport level was compared to neoclassical transport for the nominal parameters and for the experimental matched fluxes at reduced R/LTi and R/Ln, suggesting that KBM turbulence may help to prevent W accumulation in future devices.

Acknowledgement

Part of this work has been carried out within the framework of the EUROfusion Consortium and has received funding from the Euratom research and training programme 20142018 and 2019-2020 under grant agreement No 633053. The views and opinions expressed herein do not necessarily reflect those of the European Commission or the ITER Organization. The authors acknowledge access to the EUROfusion High-Performance Computer (Marconi-Fusion) through EUROfusion. Centre de Calcul Intensif d'Aix-Marseille is acknowledged for granting access to its high-performance computing resources.

References

1. A Kallenbach et al, PPCF **47,** B207 (2015)
2. A Peeters, et al, CPC **180**, 2650 (2009)
3. J Garcia, et al., Nucl. Fusion 53, 043023 (2013)
4. J Citrin, et al., Plasma Phys. Contr. Fusion 57, 014032 (2015)
5. S Moradi, et al, Nucl. Fusion 54, 123016 (2014)
6. N Kumar, et al, NF **61**, 036005 (2021)
7. 7. T. Dannert et al, POP **12**, 072309 (2005)
8. C Bourdelle, et al, POP **14**, 112501 (2007)
9. Citrin J. 2019 Qualikiz saturation rule (https://gitlab.com/ qualikiz-group/QuaLiKiz-documents/-/blob/master/reports/saturation_rule.pdf)